Available online at www.sciencedirect.com
ScienceDirect
International Journal of Thermal Sciences 48 (2009) 922–935
International Journal of Thermal Sciences
www.elsevier.com/locate/ijts

Numerical investigation of local entropy production rate of a finned oval tube with vortex generators

J. Herpe [a,b,*], D. Bougeard [a], S. Russeil [a], M. Stanciu [b]

[a] *École des Mines de Douai, Département Énergétique Industrielle, 941, Rue Charles Bourseul, BP 10838, 59508 Douai Cedex, France*
[b] *Formerly at Valeo Engine Cooling, 8, rue Louis Lormand, ZA de l'Agiot, BP 517, Le Mesnil Saint Denis Cedex, 78321 La Verrière, France*

Received 26 September 2007; received in revised form 12 July 2008; accepted 13 July 2008

Available online 30 August 2008

Abstract

The present paper analyzes the entropy production rate induced by longitudinal vortex generators punched on the fins of a compact heat exchanger. The flow is assumed to be three-dimensional, unsteady and laminar. The entropy production rate due to heat fluxes and drag forces is studied by means of finite volume methodology. The heat conduction in the fin is also taken into account and hence the induced thermal entropy production is also evaluated in the fin. The effects of the fin efficiency (factor *Fi*) and of the angle β of the vortex generator are evaluated for the volumetric entropy production rate in the fin and in the flow field. The integration over the whole domain enables to define the entropy production number N_{S1}. The relevance of this exchanger global criterion is illustrated for a specific technical requirement. The results show that the volumetric entropy production rate is predominant in the strong flow gradient zones. These zones correspond to the outer surface of the longitudinal vortex and to the thinning zone of the boundary layer (down-wash zone). This entropy production increases with *Fi* and β. In the fin the entropy production decreases with *Fi*. It is shown that the Bejan number (*Be*) is close to unity, which means that the global entropy production rate due to heat transfer is predominant in the flow field. The effectiveness of the heat exchanger increases with *Fi* and β, which corresponds to an increase of the Number of Transfer Unit NTU, but a decrease of N_{S1}.

Keywords: Longitudinal vortex; Delta winglet; Entropy production; Heat exchanger; CFD

1. Introduction

In order to assess a quantitative estimation of heat transfer performance of a finned tube heat exchanger, various approaches based on the first law of thermodynamics have been developed. Among them one can retain the Number of Transfer Units methodology ($\mathrm{NTU} = \mathrm{UA}/(\dot{m}C_p)_{\min}$). All the influent parameters like the heat transfer surface and the surface efficiency are taken into account in the global conductance coefficient UA. When focusing on the air side, the conjugate heat transfer is contained in the fin efficiency η and in the mean heat transfer coefficient $\bar{h}$. However, the modeling of $\eta\bar{h}$ by semi-empirical formula or even by numerical simulation estimation is rather complex for industrial fin shapes.

Other approaches based on the second law of thermodynamics can be found in literature. Bejan [1] has greatly contributed to the introducing the use of entropy analysis in heat exchanger design. Sekulic [2,3] has organized in a hierarchy the most common heat exchangers. Yilmaz [4] has summed up most of criteria based on the second law, and among them the entropy production number. Hesselgreaves [5] in particular has focused on the way to define the entropy production number. He has recommended to define the entropy production number N_{S1} as the entropy production rate $\dot{S}$ divided by Q/T, since "*the heat flow characterizes the raison d'être of the exchanger*". Academic cases like co-current or counter-current heat exchangers have been studied. By considering only the thermal contribution of entropy production, one remarks that for design cases in which the heat load Q is fixed, the entropy production number N_{S1} decreases monotonically as the effectiveness or NTU increases.

* Corresponding author. Tel.: +33 (0) 3 27 71 23 92; fax: +33 (0) 3 27 71 29 15.
E-mail address: herpe@ensm-douai.fr (J. Herpe).

1290-0729/$ – see front matter
doi:10.1016/j.ijthermalsci.2008.07.006

Nomenclature

A	surface	m^2
C_p	specific heat capacity at constant pressure	$J\,kg^{-1}\,K^{-1}$
C_f	friction coefficient	
$\bar{h}$	mean convective heat transfer coefficient	$W\,m^{-2}\,K^{-1}$
h^*	fin pitch	m
h	dimensionless fin pitch	
k	thermal conductivity	$W\,m^{-1}\,K^{-1}$
L^*	fin length	m
L	dimensionless fin length	
l^*	winglet length	m
l	dimensionless winglet length	
$\dot{m}$	mass flow rate	$kg\,s^{-1}$
N_β	number of finned oval tube elements for a heat exchanger	
p	pressure	Pa
q	heat flux density	$W\,m^{-2}$
Q	heat load of a heat exchanger	W
$\dot{S}'''$	volumetric entropy generation rate	$W\,m^{-3}\,K^{-1}$
$\dot{S}$	entropy generation rate	$W\,K^{-1}$
$\dot{S}'$	cross sectional entropy generation rate	$W\,m^{-1}\,K^{-1}$
T	temperature	K
UA	global conductance	$W\,K^{-1}$
u, v, w	velocity components	$m\,s^{-1}$
u_{in}	inlet velocity	$m\,s^{-1}$
V	volume	m^3
x, y, z	Cartesian coordinates	m
W^*	fin width	m
W	dimensionless fin width	

Greek symbols

β	delta winglet angle with respect to the main flow direction	°
ν	kinematic viscosity	$m^2\,s^{-1}$
ρ	density	$kg\,m^{-3}$
Φ	heat load of a finned oval tube element	W
δ^*	fin thickness	m
ε	heat exchanger effectiveness	
η	fin efficiency	
Λ	aspect ratio of the winglet	

Subscripts

f	fluid
i	vector component
in	inlet
max	maximum
min	minimum
out	outlet
s	solid
th	thermal
v	viscous

Dimensionless numbers

$Bi = \frac{\bar{h}\delta^*}{k_s}$ Biot number

$Be = \frac{S_{th,f}}{S_{th,f}+S_{v,f}}$ Bejan number

$Fi = \frac{k_s\delta^*}{k_f h^*}$ fin efficiency parameter

$Re = \frac{u_{in}h^*}{\nu}$ Reynolds number

$Nu = \frac{h^*\bar{h}}{k_f}$ Nusselt number

$N_{S1} = \frac{T_{f,in}\cdot\int S'''\,dV}{\Phi}$ entropy production number

NTU number of transfer units

Notations

DW down-wash

UP up-wash

Whereas numerous second law studies on global heat exchangers are available, only few works deal with the heat exchanger fins. Poulikakos [6] has analytically studied different academic fin shapes. However, such analytical studies remain limited for industrial shapes. The numerical simulation of heat transfer phenomena in flow fields has made important progress, and nowadays Computational Fluid Dynamics (CFD) is widely used for thermal systems design. There is also a significant increase of numerical works about the entropy production rate $\dot{S}$ in different application areas, as, for example, combustion [7], porous media [8] or forced convection [9–14]. Concerning finned tube heat exchangers, Sciubba [15] has studied the influence of the inter fins space of smooth circular fins. Herpe [16] has investigated the influence on the entropy production of the delta winglet angle (with respect to the main flow direction) of a longitudinal vortex generator punched on a fin. Herpe [17] has also analyzed the entropy production of a louvered fin tube heat exchanger and has shown the existence of an optimum of the entropy production number N_{S1} depending on the inlet velocity and the angle of the louvers. Nevertheless, the first study is limited to a simple shape, the second one considers only a uniform fin temperature and the third one considers the conjugate heat transfer but does not take into account the entropy production by heat transfer conduction in the fin.

In this paper we consider the air-side characteristics of a heat exchanger made of finned oval tubes with longitudinal vortices generators. These vortices generators are delta winglets punched on the fins. A numerical study of the conjugate heat transfer of a finned oval tube element is undertaken in order to determine the thermal and the viscous entropy production fields. The first objective is to study the impact of the vortex generator on the entropy production by comparing it with the smooth fin configuration. The second one is to study the influence of the delta winglet angle β and of the fin material on the entropy production rate. The third one is to evaluate the heat exchanger criterion N_{S1} from the local entropy production rate

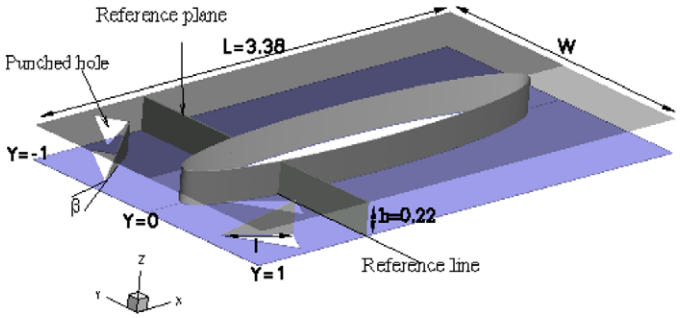

Fig. 1. Oval finned tube with two longitudinal vortex generators and definition of the plane and the line of reference used for data exploitation.

obtained by CFD and to analyze the effect of the parameters β and *Fi* on it.

2. Problem statement

Among the different passive techniques studied to increase the heat transfer, the vortex generator is one of the most attractive which can be used in the heat exchanger industry. This technique has been the subject of many works [18–27], and the physical phenomena of the longitudinal vortex due to such obstacles are well known. Chen and Fiebig [20–24] suggest using delta winglets in finned tube heat exchangers. This vortex generator disturbs locally the boundary layer and interacts with the conjugate heat transfer within the fin. The fin efficiency is locally modified and the heat exchanger performance depends on different parameters such as the angle of the delta winglet β and the fin material characterized in this paper by the fin efficiency factor *Fi* defined by Fiebig [23,24]. The conjugate heat transfer is still challenging, and is usually investigated with the heat transfer coefficient. This criterion is rather complex to determine and is still under discussion. Hence this paper proposes another way of investigation, based on the second law of thermodynamics.

The delta winglet configuration (Fig. 1) is very appropriate to illustrate the use of the second law as a criterion to characterize the conjugate heat transfer, because the longitudinal vortex generated is responsible in particular of two specific zones: the down-wash (DW) and up-wash zones (UP). Moreover, the study of a single vortices generators configuration should give useful background knowledge for more complex configurations.

Among the numerous works previously cited, the Chen configuration [20] already studied in [16] has been retained (Fig. 1). The specific relevance of the Chen configuration is that the two specific zones of the longitudinal vortex are clearly identified and isolated, as we will see in the flow description. Moreover, the Chen configuration takes into account the punched hole on the fin which has an impact on the flow topology and thus on the thermal field.

A heat exchanger is made of N_β finned oval tube elements. As all the finned oval tube elements are supposed to have the same thermodynamic behavior, the numerical investigation can be restricted to a single one. This reference finned oval tube element has the following characteristics:

- geometric features of the finned oval tube element are adimensionalized by half of the fin width W^* (see Fig. 1);
- the aspect ratio of the winglet $\Lambda = (2h^*)^2/(h^*l^*) = 2$;
- the angle of the delta winglet with respect to the main flow direction $\beta = 30°$;
- the reference fin material corresponds to a *Fi* factor equal to 500;

3. Governing equations

This configuration corresponds to a three-dimensional unsteady laminar incompressible Newtonian flow. The viscous dissipation term is neglected in energy equation. All the body forces are neglected in the momentum and energy equations. The physical properties of the fin and the fluid flow are assumed to be constant. The state equations are:

$$\frac{\partial \rho \vec{v}}{\partial t} + \vec{\nabla} \cdot (\rho \vec{v} \vec{v}) = -\vec{\nabla} p + \nabla \bar{\bar{\tau}} \tag{1}$$

$$\frac{\partial T}{\partial t} + \vec{\nabla} \cdot (\vec{v} T) = \frac{1}{(\rho C p)_f} \vec{\nabla} . (k_f \vec{\nabla} T) \tag{2}$$

$$\frac{\partial T}{\partial t} = \frac{1}{(\rho C p)_s} \vec{\nabla} . (k_s \vec{\nabla} T) \tag{3}$$

The heat transfer at the solid–fluid interface is modeled by the Fourier law:

$$q = k \frac{\partial T}{\partial z}\bigg|_{\text{wall}} \tag{4}$$

In order to calculate the volumetric entropy production rate, a direct method [28] which consists in directly solving the source terms of the transport equation of entropy is chosen. It is a post-processing methodology, where for each time step the thermal and flow fields are resolved. Then, knowing the thermal and velocity gradients, the source terms can be evaluated. Indeed, according to Moore [29] and Adeyinka [30] the volumetric entropy generation rate in the fluid is composed of viscous and thermal dissipations:

$$\dot{S}'''_f = \dot{S}'''_{v,f} + \dot{S}'''_{\text{th},f} \tag{5}$$

The first term, which is the volumetric entropy production rate due to direct viscous dissipation, can be written as follows:

$$\begin{aligned} \dot{S}'''_{v,f} = \frac{\mu}{T} \Bigg[& 2 \left\{ \left(\frac{\partial u}{\partial x} \right)^2 + \left(\frac{\partial v}{\partial y} \right)^2 + \left(\frac{\partial w}{\partial z} \right)^2 \right\} \\ & + \left(\frac{\partial u}{\partial y} + \frac{\partial v}{\partial x} \right)^2 + \left(\frac{\partial u}{\partial z} + \frac{\partial w}{\partial x} \right)^2 \\ & + \left(\frac{\partial v}{\partial z} + \frac{\partial w}{\partial y} \right)^2 \Bigg] \end{aligned} \tag{6}$$

The second term, which is the volumetric entropy production rate due to heat transfer, can be expressed as:

$$\dot{S}'''_{\text{th},f} = \frac{k_f}{T^2} \left[\left(\frac{\partial T}{\partial x} \right)^2 + \left(\frac{\partial T}{\partial y} \right)^2 + \left(\frac{\partial T}{\partial z} \right)^2 \right] \tag{7}$$

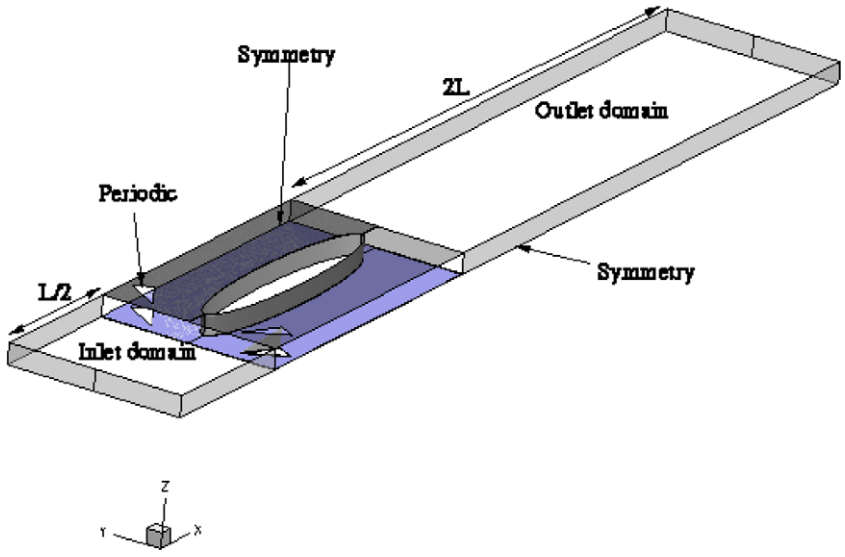

Fig. 2. Numerical domain and boundary conditions.

In the fin the volumetric entropy production rate is only due to the heat flux:

$$\dot{S}'''_{\mathrm{th},s} = \frac{k_s}{T^2}\left[\left(\frac{\partial T}{\partial x}\right)^2 + \left(\frac{\partial T}{\partial y}\right)^2 + \left(\frac{\partial T}{\partial z}\right)^2\right] \tag{8}$$

The entropy generation rate in a given volume is then computed by integrating all the local contributions:

$$\dot{S} = \int_V \dot{S}''' \, dV \tag{9}$$

The volume V corresponds to the volume of the fin and/or the volume of the air domain contained between the fins. The inlet and outlet computational domains (Fig. 2) are not taken into account in the $\dot{S}$ evaluation, because their contribution is negligible.

4. Numerical modeling

As stated in the foregoing paragraph, the entropy production terms are determined from the temperature and velocity fields. As a consequence, the accuracy of the entropy production field calculation is directly linked to the quality of the temperature and velocity fields obtained by the CFD analysis. Several previous works [20–22,25] have enforced the use of laminar three-dimensional numerical simulations for finned oval tube heat exchangers at low Reynolds numbers. In particular Chen and co-workers have performed accurate comparison between their numerical results and experimental data (see references in [20] for more details) in order to validate their CFD investigations.

Our computational results, obtained by using the numerical method described in following paragraphs, have been successfully compared to Chen's numerical data. Indeed numerical/experimental comparisons of the temperature distribution on the fin and span-averaged pressure distribution across the finned oval tube element have shown perfect agreement, see, for example, Fig. 3. Due to lack of space in the paper, the complete validation procedure is not reported here but can be seen in [32].

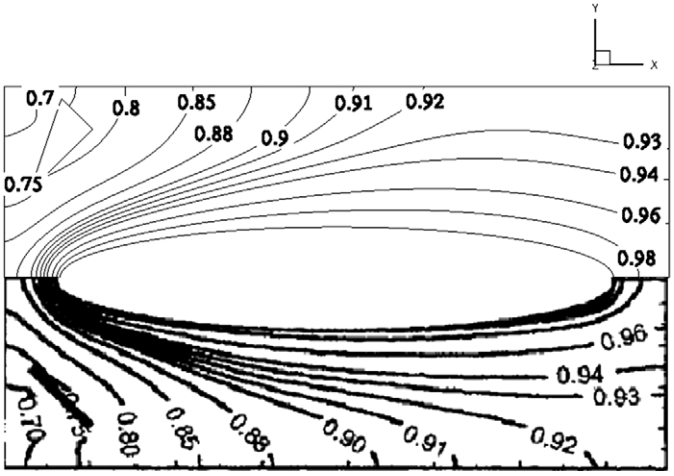

Fig. 3. Dimensionless temperature distribution on the fin, $(T - T_{\mathrm{in}})/(T_{\mathrm{tube}} - T_{\mathrm{in}})$: present study (upper), Chen results [20] (lower).

4.1. Numerical procedure

The conservative equations are solved using the Fluent commercial solver [31]. The volumetric entropy production rate obtained by post-processing is calculated with specifically developed subroutines.

The equations have been linearized in an implicit form and solved sequentially. The SIMPLEC algorithm has been used for the pressure-velocity coupling. The pressure interpolation scheme has been chosen to be a second order upwind scheme. The momentum equation has been discretized with a power law scheme and the energy equation with a second order scheme. In order to calculate the convection and diffusion terms constituted by a derivative function, the Green Gauss theorem has been used. The derivative is a function of the physical value at

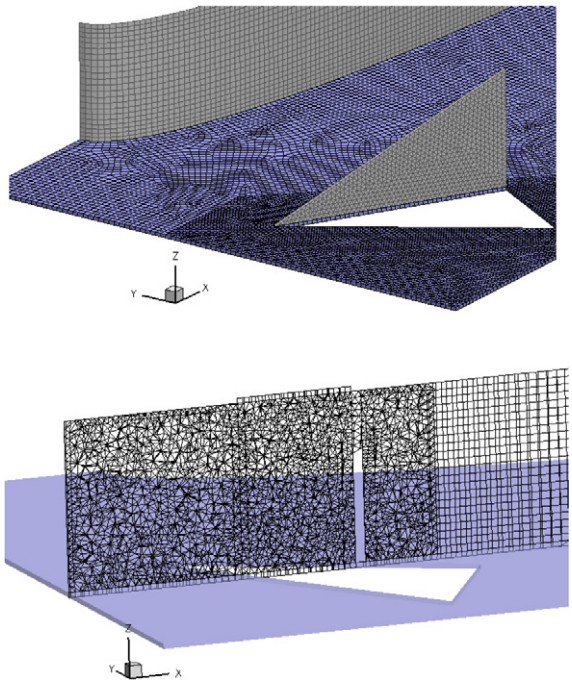

Fig. 4. Detailed view of the surface mesh and the volume mesh around a delta winglet.

the cell face. This face value is calculated as the arithmetic average of the values at the neighboring cell centers.

4.2. Computational domain and boundary conditions

The computational domain is shown in Fig. 2. The x-axis is aligned with the main flow direction. The y-axis is the cross direction, and the z-axis corresponds to the direction perpendicular to the fins. The upstream numerical domain has an $L/2$ length and the downstream numerical domain has a $2L$ length.

The boundary conditions are the following:

- At the inlet, the temperature is set to 293 K and the velocity is specified such as it corresponds to a Reynolds number equal to 300.
- At the outlet the atmospheric pressure is fixed.
- The punched holes in the fins are assumed to be periodic boundary conditions in the z-direction.
- A heat flux equal to zero is fixed on the outer side of the fins.
- On the left and right sides of the finned oval tube element symmetric boundary conditions are set.
- The thickness of the wall tube is not taken into account. As we focus only on the air-side performances, the convective heat transfer in the tube, the conduction in the tube wall and the contact resistance at the fin tube junction are not considered and the tube outer surface is assumed to be isothermal.

In order to optimize the mesh size and quality, the mesh domain is divided in three zones. The first one is localized around the delta winglets (Fig. 4). It is made of tetrahedral elements and is refined near the wall. The second zone takes into account the rest of the air side. Hexahedral elements have been used. The third one corresponds to the fin. The material of the fin corresponding to $Fi = 500$ is aluminium. In this case the Biot number is small with respect to unity. Thus the heat conduction is assumed to be two-dimensional in the fin. Therefore the mesh in the fin contains only a hexahedral cell in the thickness.

The mesh quality as required in [31] is such as the equiangle size factor and aspect ratio factor of the cells are respectively below 0.85 and 5. The results grid independency has been assessed in [32] by comparing three meshes with 1.6, 2.8 and 4.5 million of cells. Skin friction coefficient values, Nusselt numbers, local and global entropy production rates have been shown to converge with the number of mesh elements (see Table 1). Finally the finest mesh has been chosen for the present numerical study.

4.3. Temporal discretization

Because of the vortex shedding downstream the tube and the unsteadiness of the longitudinal vortices (Fig. 5 (a) and (b)), an unsteady numerical formulation is necessary. A first order implicit scheme is chosen. The monitoring of the flow velocity shows that the wake downstream the tube and the secondary flow generated by the vortex generators are unsteady periodic structures. The necessary time step considered to capture the velocity and temperature fluctuations is 8×10^{-5} s, corresponding to 30 samples per period. The initial conditions are such that dynamic and thermal fields are uniform on the computational domain at the initial time step. Equations for continuity, momentum and energy have been solved until the establishment of the periodic oscillations and also the convergence of the residual criteria is reached [31] for each time step. The residual criteria are set to 10^{-6} for continuity equation and 10^{-8} for momentum and energy.

The flow unsteadiness is responsible of temperature and velocity fluctuations, hence of entropy production fluctuations. As the outlet and the inlet domain are not considered for the evaluation of $\dot{S}$, the periodic evolution of $\dot{S}$ in the process of time is supposed to correspond only to the unsteadiness of the longitudinal vortex confined between the fins. The arithmetic time average of the entropy production rates, and of all the other physical values considered here, is based on the two last calculated periods of the established periodic phenomena observed. Anyway, the time fluctuations of the entropy production are negligible with regards to the variation of entropy production due to a parametric modification. In fact, the variations of $\dot{S}$ around the averaged value are below 0.01% for all the configurations studied, which is significantly smaller than the parametric variations studied in the following sections.

5. Results and discussion

5.1. Flow description

The two delta winglets on the fin generate a secondary flow on both sides of the tube. This secondary flow is composed of a

Table 1
Mesh sensitivity

Mesh size (number of cells in million)	ESMS(m)/ESMS($m=4.5$)	$Nu(m)/Nu(m=4.5)$	$C_f(m)/C_f(m=4.5)$	$\dot{S}(m)/\dot{S}(m=4.5)$
$m=1.6$	2.6	1%	0.8%	0.6%
$m=2.8$	1.7	0.4%	0.2%	0.3%
$m=4.5$	1	0%	0%	0%

ESMS = Element Surface Mesh Size.

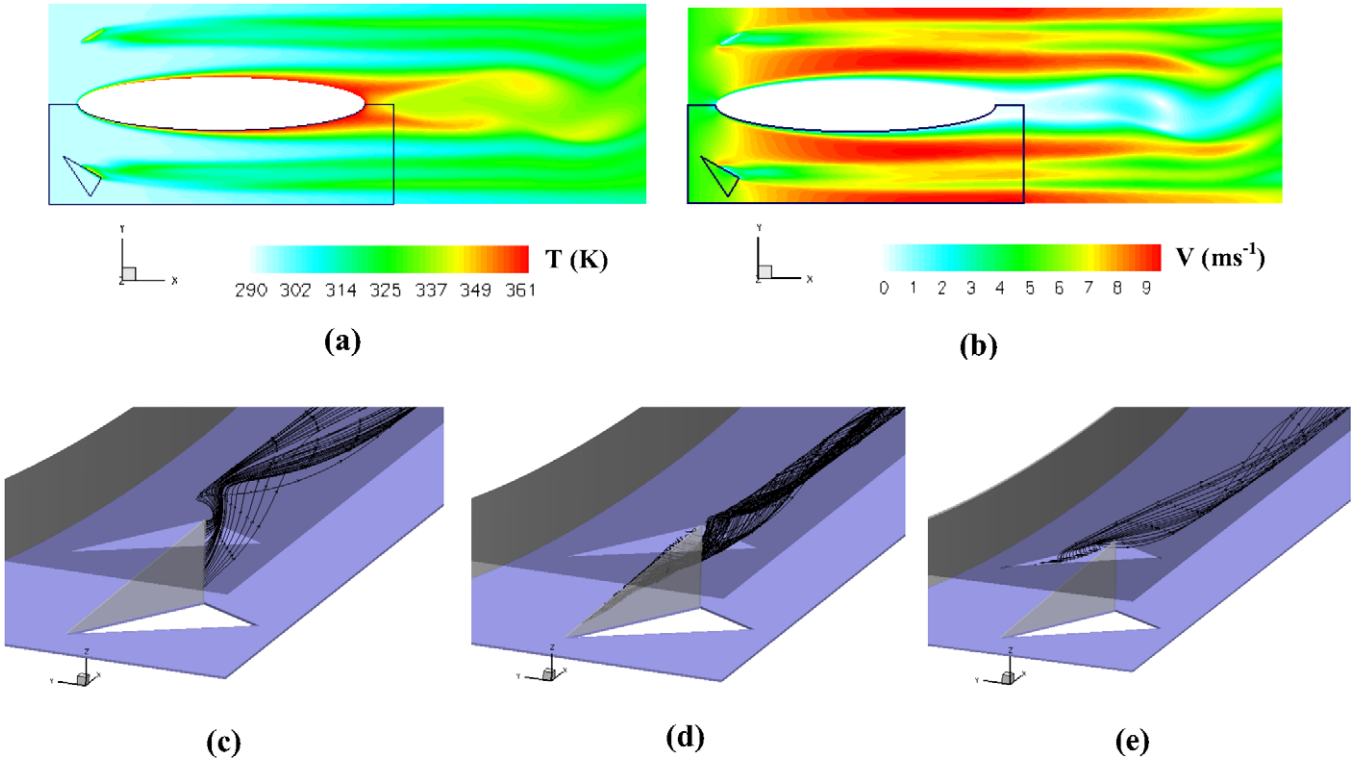

Fig. 5. (a)–(b) Contours of temperature (K) and velocity (m s^{-1}) in the mid plane describing the wake structure downstream the tube. (c) Streamlines starting from the trailing edge of the delta winglet. (d) Streamlines starting from the leading edge of the delta winglet. (e) Streamlines passing through the punched holes.

main longitudinal vortex and secondary vortices. The main vortex is due to the roll-up of the streamlines separating from the leading edge and the trailing edge of the winglet. The trailing edge streamlines (Fig. 5(c)) wrap the leading edge streamlines (Fig. 5(d)), constituting the core of the main vortex. The streamlines coming through the punched hole ahead the delta winglet, also participate to the wrapping (Fig. 5(e)) of the core of the main vortex.

The horseshoe vortex, which could appear ahead the tube, for such junction flow configurations, is not observed due to the fin pitch, the length of the fin upstream the tube and the Reynolds number [33]. Hence the flow topology is only characterized by the two longitudinal vortices previously described. The delta winglet is orientated such as the longitudinal vortices move away from the tube, but they do not merge with the symmetric neighboring vortices generated by the periodical element because the length of the fin is small.

The longitudinal vortex induced by the delta winglet greatly modifies the velocity and the temperature fields and therefore the heat transfer rates. This secondary flow is responsible of (Fig. 6):

(1) The thinning of the thermal boundary layer in regions called down-wash zones (see DW1 and DW2) which results in a significant increase of the heat transfer and of the wall viscous friction, respectively characterized by the Nusselt number Nu and the skin friction coefficient C_f, which are plotted (Fig. 6) on the reference line define in Fig. 1.
(2) On the contrary, the thickening of the thermal boundary layer is noticed in regions called up-wash zones (UP1 and UP2) where wall heat flux and friction are markedly reduced.

5.2. Entropy production

First, the global entropy production of the element is investigated. In a second step, the entropy production in cross-sections along the flow passage is examined. Finally, the local entropy production in the reference plane (defined in Fig. 1) is studied.

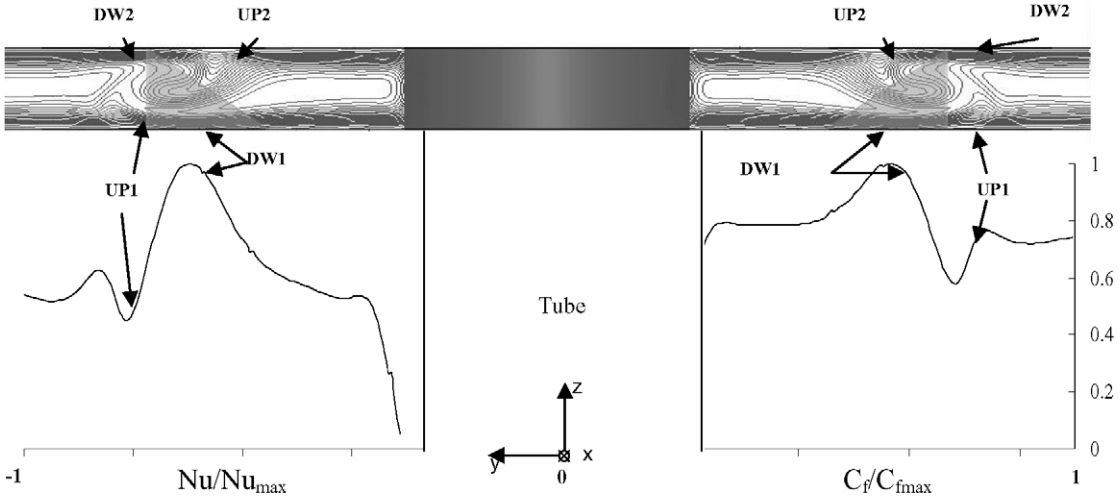

Fig. 6. Isotherm in the reference plane. Nusselt and skin friction evolution on the reference line.

Table 2
Winglet impact on the thermal entropy production rate

Entropy production components	Smooth fin [%]	Delta winglet $\beta = 30°$ [%]
$\dot{S}_{\text{th},s,x}/\dot{S}_{\text{th},s}$	24.7	24.9
$\dot{S}_{\text{th},s,y}/\dot{S}_{\text{th},s}$	75.3	74.5
$\dot{S}_{\text{th},s,z}/\dot{S}_{\text{th},s}$	0	0.6
$\dot{S}_{\text{th},f,x}/\dot{S}_{\text{th},f}$	2.0	3.8
$\dot{S}_{\text{th},f,y}/\dot{S}_{\text{th},f}$	6.3	12.3
$\dot{S}_{\text{th},f,z}/\dot{S}_{\text{th},f}$	91.6	83.8

5.2.1. *Part of each term of entropy production in the finned oval tube element*

In this paragraph the entropy production in a smooth finned oval tube element is compared to the entropy production for a finned oval tube with delta winglets. Delta winglets have an impact on the global entropy production, due to the modification of the flow and thermal fields as previously described. As expected, the entropy production due to direct dissipation increases by punching the winglet on the fin. But it is worth to note that, for both configurations, the Bejan number is very close to unity, which means that heat transfer irreversibilities prevail over fluid friction irreversibilities. Thus in the following sections, our analysis is focused only on the thermal part.

By punching the winglet on the fin, the entropy production in the flow $\dot{S}_{\text{th},f}$ increases of 8% and the entropy production in the fin $\dot{S}_{\text{th},s}$ increases of 37%. The part of $\dot{S}_{\text{th},s}$ increases from 10.5% to 13.0% (Table 2), and therefore the entropy production rate in the fin has to be taken into account in order to estimate correctly the overall entropy production of the finned oval tube element.

The thermal entropy production term in the flow field and in the fin is now studied analyzing each production due to the thermal gradients in the x-direction, in the y-direction and in the z-direction:

$$\dot{S}'''_{\text{th}} = \dot{S}_{\text{th},s,x} + \dot{S}_{\text{th},s,y} + \dot{S}_{\text{th},s,z} = \frac{k_f}{T^2}\left(\frac{\partial T}{\partial x}\right)^2 + \frac{k_f}{T^2}\left(\frac{\partial T}{\partial y}\right)^2 + \frac{k_f}{T^2}\left(\frac{\partial T}{\partial z}\right)^2$$

Each contribution to the global entropy production in each direction ($\dot{S}_{\text{th},s,x}$, $\dot{S}_{\text{th},s,y}$, $\dot{S}_{\text{th},s,z}$) is summarized in Table 2.

The parts of $\dot{S}_{\text{th},s,x}$ and $\dot{S}_{\text{th},s,y}$ correspond respectively to around 25% and 75% of the total entropy production $\dot{S}_{\text{th},s}$ in the smooth fin. This ratio does not significantly change when punching the delta winglet. The thermal gradients are more important in the y-direction. In fact, the isotherms spread all around the oval tube and are more concentrated near the tube. As the heat conduction in the fin is supposed two-dimensional, $\dot{S}_{\text{th},s,z}$ is zero in the fin. In the delta winglets which are perpendicular to the fin, the z contribution is negligible.

When punching a winglet, the flow topology is modified. Hence the distribution of thermal entropy production $\dot{S}_{\text{th},f}$ is significantly changed: $\dot{S}_{\text{th},f,x}$ and $\dot{S}_{\text{th},f,y}$ are multiplied by almost two when punching the winglet. Consequently the z contribution is reduced from 91.6% to 83.9% (Table 2) but remains the most important one.

5.2.2. *Cross sectional entropy production due to heat transfer in the flow*

The cross sectional integration of the thermal entropy production in the flow ($\dot{S}'_{\text{th},f}$) due to the two delta winglets is plotted and compared with the smooth fin results (Fig. 7). The values of thermal entropy production are adimensionalized by the value of $\dot{S}'_{\text{th},f,z}$ at the fin leading edge ($S_{\text{th},f,\max}$) which is the maximum value in the domain.

By considering the smooth fin one remarks a single peak appearing upstream the tube for $\dot{S}'_{\text{th},f,x}$ and $\dot{S}'_{\text{th},f,y}$ which is due to the modification of the flow direction (curvature of the streamlines) upstream the stagnation point on the tube. Because of the flow topology around the winglets, there are strong thermal gradients and thus a significant variation of entropy production. Also, an important increase of $\dot{S}'_{\text{th},f,x}$ and $\dot{S}'_{\text{th},f,y}$ are expected when a winglet is punched on the fin. Indeed, two peaks occur for the cross sectional distribution of $\dot{S}'_{\text{th},f,x}$ and $\dot{S}'_{\text{th},f,y}$ (Fig. 7). The first one appears upstream the tube, similarly to the smooth fin case, but enlarged by the presence of the winglet. The second one appears at the trailing edge of the winglet. For

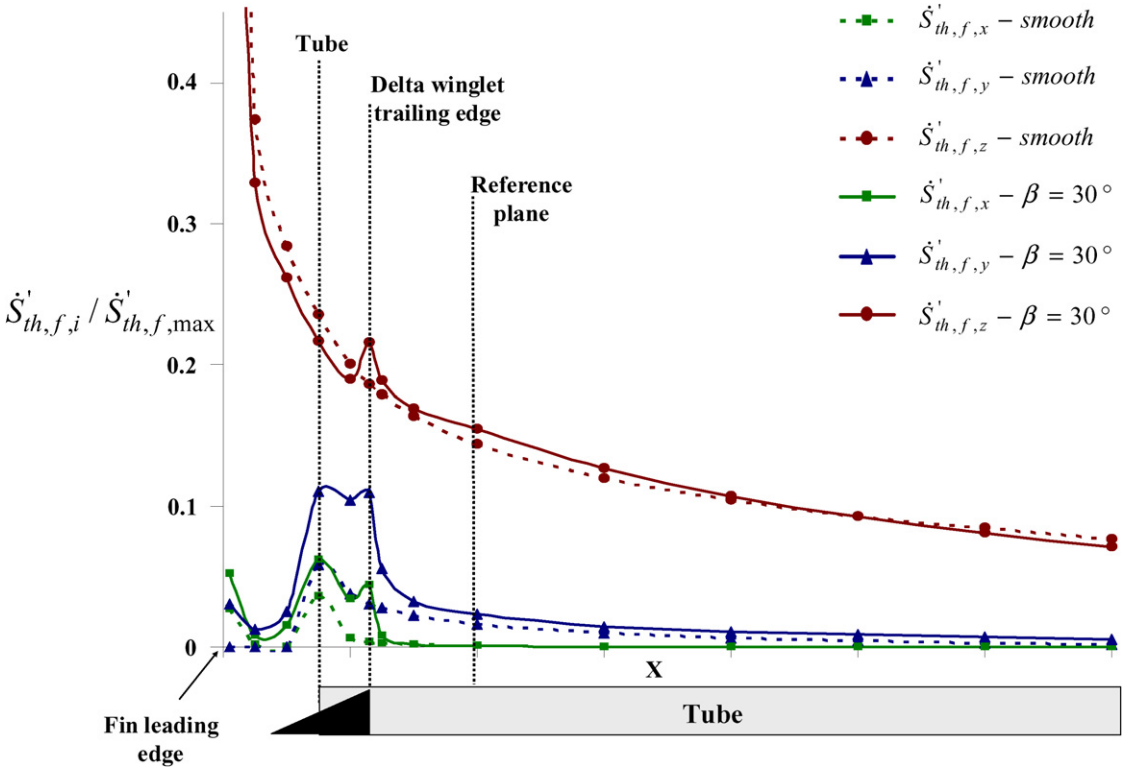

Fig. 7. Cross-sectional integration of $\dot{S}'''_{\mathrm{th},f,i}$ (W K^{-1} m^{-3}) along the heat exchanger element.

$\dot{S}'_{\mathrm{th},f,z}$ only the second peak is noticed. The slight decrease of z contribution (with regard to the smooth fin) which is noticed at the punched hole placed upstream the delta winglet, takes part in the global decrease of the z contribution noticed in Table 2.

Downstream the trailing edge of the delta winglet, cross sectional values of the x contribution $\dot{S}'_{\mathrm{th},f,x}$ decrease and reach similar values as for the smooth fin. On the other hand, the values of $\dot{S}'_{\mathrm{th},f,y}$ and $\dot{S}'_{\mathrm{th},f,z}$ decrease, but do not reach the values of the smooth fin because of the development of the secondary flow in the plane y–z. The behavior of the y and z contributions, which prevail over the x part, is explained more in details in the following section.

5.2.3. *Volumetric entropy production rate due to heat transfer in the flow*

The contours (Fig. 8) of the local thermal entropy production rate and the isotherms, are plotted in the reference plane, downstream the delta winglet (Fig. 1), where the longitudinal vortex is clearly observed. As the x contributions of the thermal entropy production rate is very small in comparison to the two others contributions downstream the delta winglets (Fig. 7), it does not play a significant role in the entropy production in the longitudinal vortex and is not considered in the following local description. Fig. 8 (a) and (b) corresponds to the smooth fin case and Fig. 8 (c) and (d) corresponds to the fin with delta winglets.

The increase of $\dot{S}'''_{\mathrm{th},f,z}$, for the finned oval tube with respect to the smooth fin is essentially due to the modification of the thermal boundary layer induced by the vortex generator. For example, in the down-wash zones near the fin surface (DW1 and DW2 zones in Fig. 8(d)), the boundary layer is thinned by the longitudinal vortex structure. Therefore the isotherms near the wall are plucked, the thermal gradients in the z-direction increase and the volumetric entropy production rate due to heat transfer increases. On the contrary, in the up-wash zones (UP1 and UP2 zones in Fig. 8(d)), the boundary layer is thickened and thus the corresponding entropy production locally decreases.

If the maximum of $\dot{S}'''_{\mathrm{th},f,z}$ clearly occurs near the walls (DW1 and DW2), there is also a thermal gradient in the outer surface of the longitudinal vortex. Indeed, due to its roll up in the flow field, above DW1 (near the lower fin surface) the "cold layer" of fluid is approximately equal to 300 K and the fluid in the vortex core is at a higher temperature level around 322 K. The corresponding induced thermal gradients are responsible for the thermal entropy production in the z-direction near the outer surface of the vortex core.

The flow topology produced by the vortex generator is also responsible of an increase of the thermal entropy production rate in y-direction (Fig. 8(c)). The modification of the fin boundary layer does not strongly modify the value of $\dot{S}'''_{\mathrm{th},f,y}$ near the fins neither in the tube vicinity. But the punching of the winglet is clearly responsible of an increase of the y contribution in the core of the flow (Fig. 8 (a) and (c)). In fact, the distortion of the isotherms in the up-wash zones (UP1 and UP2) induces thermal gradients in the y-direction, which are responsible of a production of $\dot{S}'''_{\mathrm{th},f,y}$.

To summarize, the entropy production appears as a useful mean to analyze the heat transfer everywhere in the fluid

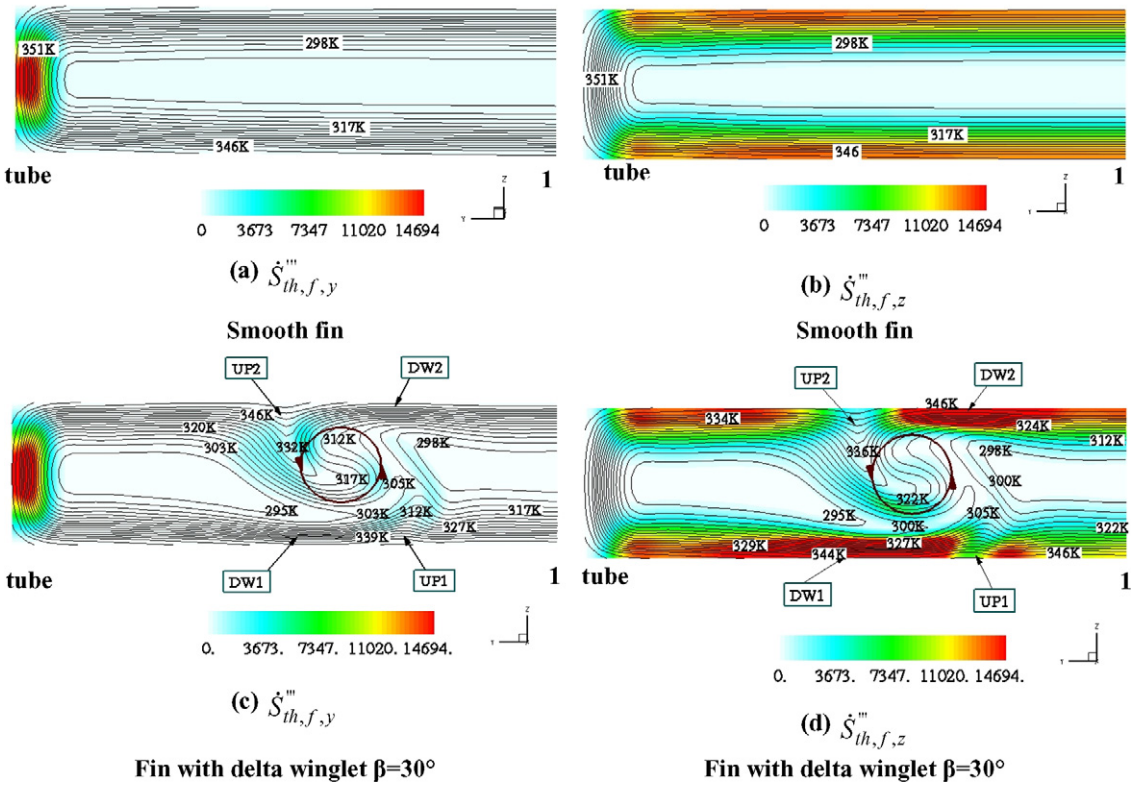

Fig. 8. Contour of volumetric entropy production in the fluid ($\mathrm{W\,m^{-3}\,K^{-1}}$) and isotherms (K) in the reference plane. The left-hand side corresponds to the y contribution. The right-hand side corresponds to the z contribution.

Table 3
Influence of β on the thermal and viscous entropy production rates

Entropy production components	Delta winglet $\beta = 20°$	Delta winglet $\beta = 30°$	Delta winglet $\beta = 45°$
$\dot{S}_{v,f,\beta}/\dot{S}_{v,f,\mathrm{smooth}}$	1.17	1.27	1.40
$\dot{S}_{\mathrm{th},f,\beta}/\dot{S}_{\mathrm{th},f,\mathrm{smooth}}$	1.05	1.08	1.09
$\dot{S}_{\mathrm{th},s,\beta}/\dot{S}_{\mathrm{th},s,\mathrm{smooth}}$	1.30	1.37	1.42

domain. In fact, the near-wall zones of high heat transfer rates (DW zones) have been identified as well as the mixing heat transfer process in the longitudinal vortex shear layer.

Also, it is worth to note that the entropy production rate does not just represent a wall criterion as the heat transfer coefficient $\bar{h}$ or the Nusselt number. Moreover, it is not necessary to define any reference temperature, which might be difficult to determine for complex shapes. Finally, the global characterization of the finned oval tube element can be obtained by a single integration of all the local contributions for the entropy criterion, whereas the finned oval tube heat transfer coefficient is an averaged value.

5.3. Influence of β and Fi on entropy production

In this section the influence of the angle of the delta winglet β and the factor *Fi* are studied. For each parameter a global evaluation of entropy production, as well as local information, are presented.

5.3.1. Influence of the angle of the winglet β

In this paragraph the influence of the three following angles is studied: $\beta = 20°$, $\beta = 30°$ and $\beta = 45°$. The physical phenomena previously described in Section 5.2 are amplified with the increase of β. It is shown that the power dissipated increases with the angle β (+4% from $\beta = 20°$ to $\beta = 30°$ and +7% from $\beta = 20°$ to $\beta = 45°$). Both entropy production due to flow friction ($\dot{S}_{v,f}$) and heat transfer in the fluid ($\dot{S}_{\mathrm{th},f}$) and in the fin ($\dot{S}_{\mathrm{th},s}$) increase with the angle β (see Table 3). It is worth to note that the viscous contribution to entropy production $\dot{S}_{v,f}$ increases by 23% from the case $\beta = 20°$ to the case $\beta = 45°$, but the entropy production due to heat transfer remains predominant. The Bejan number is still close to the unity.

First, the case of fin entropy production $\dot{S}_{\mathrm{th},s}$ is considered. The strength of the longitudinal vortex increases with β and as a consequence, wall heat fluxes are stronger and the fin is locally more cooled. The conjugate heat transfer is responsible of an increase of local thermal gradients in the fin and of the entropy production. Accordingly, the part of $\dot{S}_{\mathrm{th},s}$ increases with respect to the part of $\dot{S}_{\mathrm{th},f}$ (Fig. 9(a)). But for all the values of the angle β, the x- and the y-contribution of $\dot{S}_{\mathrm{th},s}$ remain roughly the same (respectively 25% and 75%).

Considering the flow field entropy production, the increase of the strength of the longitudinal vortex with β is responsible of the increase of both $\dot{S}_{v,f}$ and $\dot{S}_{\mathrm{th},f}$ close to the delta winglets and downstream them, because of the vortices development. Both have their maximum value located around the delta winglets. Moreover, on the contrary to the fin thermal entropy production, the modification of the angle β has a strong

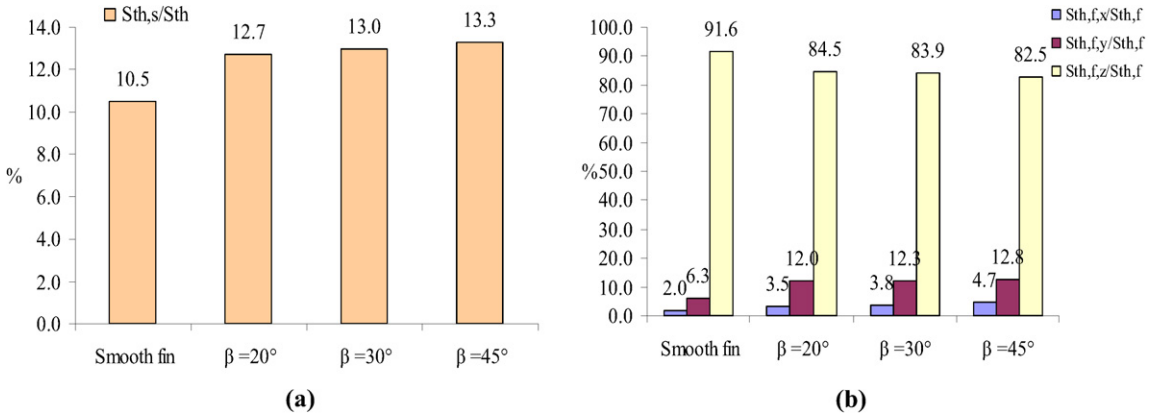

Fig. 9. (a) Ratio of the thermal entropy production in the fin $\dot{S}_{\mathrm{th},s}$ ($\mathrm{W\,K^{-1}}$) with respect to the overall thermal entropy production $\dot{S}_{\mathrm{th}}$ ($\mathrm{W\,K^{-1}}$). (b) Ratio of the contributions of thermal entropy production in the fluid.

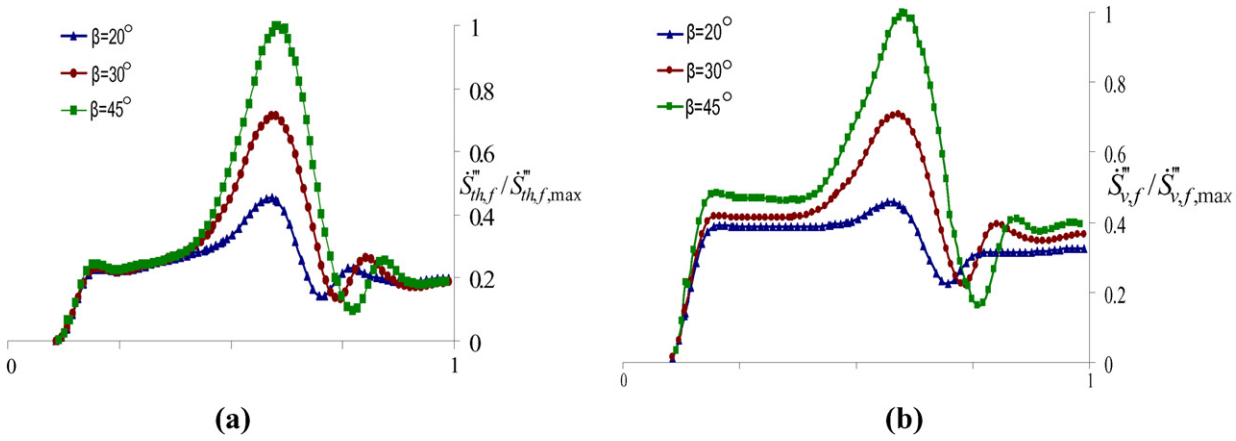

Fig. 10. Evolution of $\dot{S}'''_{\mathrm{th},f}$ (a) and $\dot{S}'''_{v,f}$ (b) on the adjacent cells of the wall along the reference line ($\mathrm{W\,m^{-3}\,K^{-1}}$).

impact on the thermal entropy production distribution in the fluid (Fig. 9(b)). It is due to the three-dimensional structure of the longitudinal vortex. The parts of $\dot{S}_{\mathrm{th},f,x}$ and $\dot{S}_{\mathrm{th},f,y}$ enlarge with increasing β and the z contribution ($\dot{S}_{\mathrm{th},f,z}$) is lower.

The local entropy production rates are described below, in the reference line and plane (defined in Fig. 1), in order to explain the local influence of the delta winglet. The volumetric entropy production rates in the cells adjacent to the wall along the reference line on the lower fin, $\dot{S}'''_{\mathrm{th},f}$ and $\dot{S}'''_{v,f}$, are plotted in Fig. 10 (a) and (b). Both increase with the delta winglet angle β, in the down-wash zone DW1 (as well as friction coefficients and Nusselt numbers, see Fig. 6) and decrease in the up-wash zone UP1. The longitudinal vortex also impacts the core of the flow field as highlighted in Fig. 11 that represents the contours of $\dot{S}'''_{\mathrm{th},f}$ and $\dot{S}'''_{v,f}$ in the reference plane. The comparison between $\beta = 20°$ and $\beta = 45°$ is represented for both $\dot{S}'''_{\mathrm{th},f}$ and $\dot{S}'''_{v,f}$. As already mentioned, the vorticity of the longitudinal vortex increases with β. The shear stress layer is stronger in the skin of the longitudinal vortex as well as the thermal gradient, hence $\dot{S}'''_{\mathrm{th},f}$ and $\dot{S}'''_{v,f}$ increase. The outer surface of the longitudinal vortex represents an important mixing and dissipating zone of energy in the flow and the entropy production is important. All these local contributions, which increase with β, are responsible of the global increase of the entropy production.

As reported by Chen [20], the thermal performance increases with the delta winglet angle. It is shown here that this thermal performance enhancement due to the angle β, is directly related to an increase of entropy production in the flow field and in the fin.

5.3.2. *Influence of the fin efficiency parameter Fi*

The fin efficiency, which has a great importance in heat exchanger design, is directly linked to the fin thickness and fin material. Fiebig [23,24] has defined the non-dimensional factor *Fi* which takes into account both parameters. The goal of this paragraph is to evaluate the influence of *Fi* on the entropy production. The parametric study of this parameter is particularly relevant to illustrate the impact of the conjugate heat transfer on entropy production in the fin and in the fluid. For this analysis, the reference configuration having the delta winglet angle $\beta = 30°$ has been considered. The fin thickness has been fixed and three values of *Fi* have been considered: $Fi = 500$, 1000 and 5000. They respectively correspond to a fin made of aluminium, copper and a very high conduction material that corresponds to an efficiency η close to 1 [23,24].

Because of the better heat conduction, when *Fi* increases, the fin temperature tends to be uniform, the thermal gradients decrease down to zero and the entropy production rate in the fin

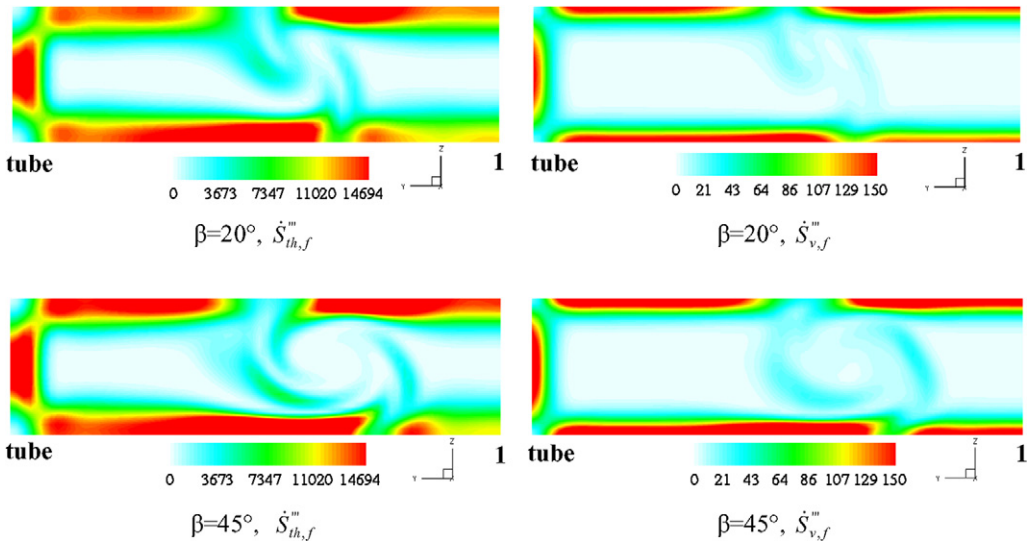

Fig. 11. Contours of entropy production in the fluid (W m^{-3} K^{-1}) due to heat flux $\dot{S}'''_{\mathrm{th},f}$ and viscous dissipation $\dot{S}'''_{v,f}$ in the reference plane.

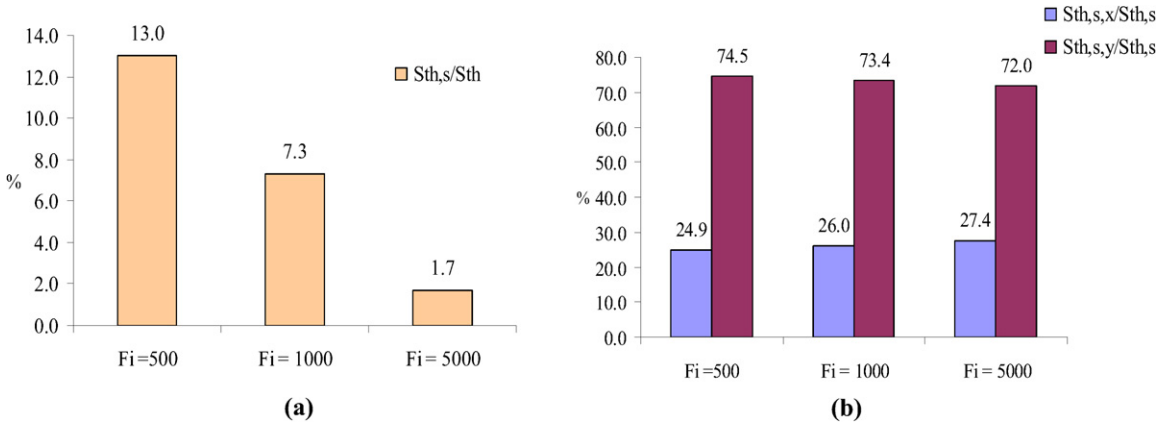

Fig. 12. (a) Ratio of the thermal entropy production in the fin $\dot{S}_{\mathrm{th},s}$ (W K^{-1}) with respect to the overall thermal entropy production $\dot{S}_{\mathrm{th}}$ (W K^{-1}). (b) Ratio of the contributions of thermal entropy production in the solid.

($\dot{S}_{\mathrm{th},s}$) also, see Fig. 12(a)). Both $\dot{S}_{\mathrm{th},s,x}$ and $\dot{S}_{\mathrm{th},s,y}$ decrease, but the decrease of the y part is greater. Indeed, the x contribution $\dot{S}_{\mathrm{th},s,x}$ slightly increases with respect to the part of $\dot{S}_{\mathrm{th},s,y}$, when Fi increases (Fig. 12(b)). Nevertheless the y contribution remains predominant (roughly 75% of $\dot{S}_{\mathrm{th},s}$). The x and y contributions to the entropy production rate in the fin are plotted in Fig. 13 for $Fi = 500$ and $Fi = 5000$. This illustrates the predominance of the y contribution and it shows that the entropy production is concentrated upstream of the tube.

As previously mentioned, the entropy production decreases down to zero in the fin when Fi increases and the temperature becomes uniform and tends to the tube temperature. Therefore, there is an increase of the thermal gradient between the fin surface and the fluid. Thus the entropy production due to heat transfer increases in the fluid. The growth rate of $\dot{S}'''_{\mathrm{th},f}$ is equal to 19% when Fi increases from 500 to 5000. This increase of entropy production appears near the wall (Fig. 14). We can notice that the entropy production also increases in the core of the vortex.

It is worth to note that the increase of thermal entropy production in the fluid is not balanced by the decrease of entropy production in the fin. As a consequence, the overall $\dot{S}_{\mathrm{th}}$ increases with Fi. Indeed, the growth rate is respectively equal to 2.6% for $Fi = 1000$ and 5.2% for $Fi = 5000$ when comparing to the case $Fi = 500$.

A better fin efficiency is shown to be responsible of a decrease of the thermal entropy production in the fin but a global increase of thermal entropy production.

5.4. Entropy production number criteria for heat exchangers

In the previous sections the evolution of the volumetric entropy production rate of a finned oval tube element has been studied for different parameters. Their effects on the conjugate heat transfer phenomena have been characterized. The local pieces of information previously obtained are, in this section, completed by a global analysis. In order to estimate the relevance of the modification (Fi or β) of a finned oval tube element on the global heat exchanger, the entropy production number

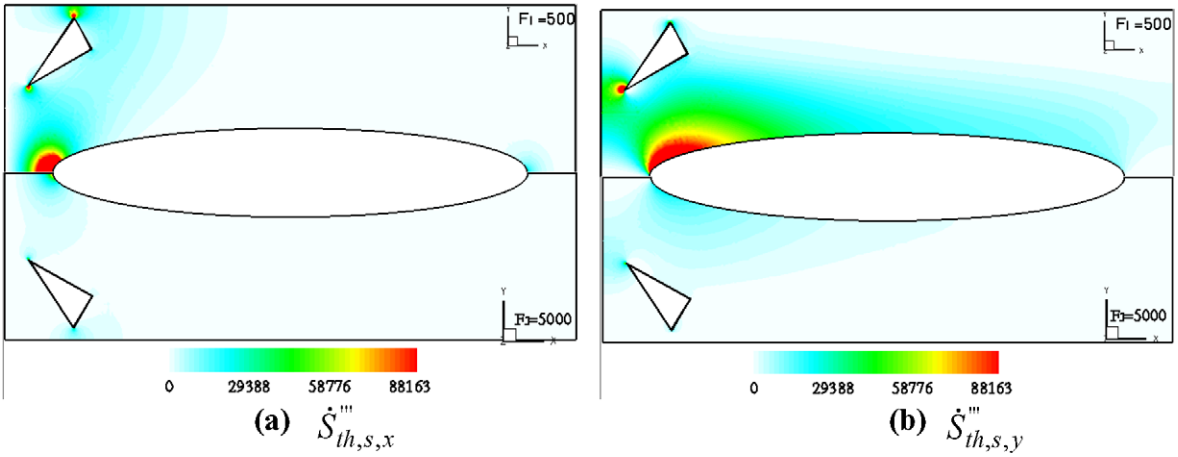

Fig. 13. Distribution of $\dot{S}'''_{\mathrm{th},s,x}$ (a) and $\dot{S}'''_{\mathrm{th},s,y}$ (b) in the bottom fin (W m^{-3} K^{-1}). Upper case $Fi = 500$, bottom case $Fi = 5000$.

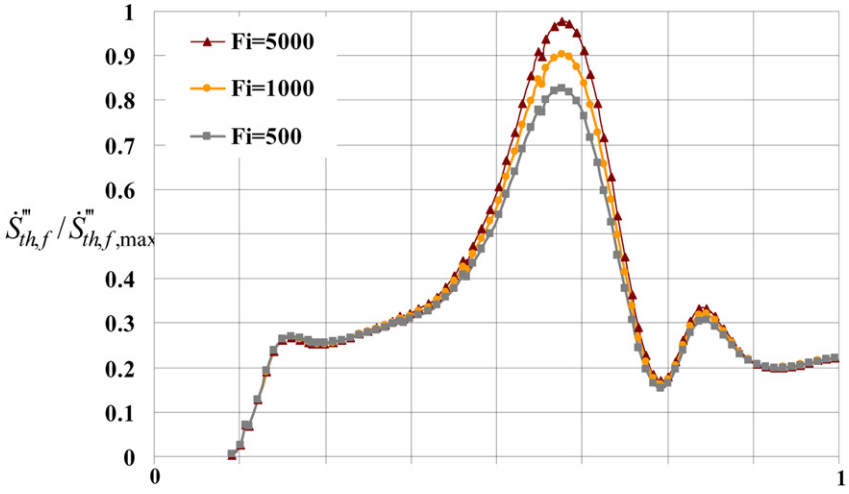

Fig. 14. Evolution of $\dot{S}'''_{\mathrm{th},f}$ (W m^{-3} K^{-1}) on the adjacent cells of the wall along the reference line.

N_{S1} is defined as a global criterion. The impact of the parametric modifications on N_{S1} is studied. The evolution of the entropy production number N_{S1} is also compared to the classical NTU methodology.

In this section the entropy production number criteria behavior is illustrated for a common technical requirement. Among several possible technical requirements available, we have chosen one to illustrate the methodology used to link local entropy production information to the global criteria N_{S1}.

As an example, four fin designs of a given heat load heat exchangers are compared. The first one corresponds to the smooth fin and the three others correspond to the three β delta winglets angles previously studied.

As in previous sections, the tube thickness is not taken into account, the tube temperature is fixed and the thermal contact resistance between the fin and the tube is not considered. Thus we only take into account the air side resistance for the NTU estimation. The averaged heat transfer coefficient of the finned oval tube is then evaluated by means of the logarithm difference temperature ΔT_{lm} [34]:

$$\mathrm{NTU} = \frac{\Phi}{(\dot{m}C_p)_f \Delta T_{lm}} \tag{10}$$

with

$$\Delta T_{lm} = \frac{T_{f,\mathrm{out}} - T_{f,\mathrm{in}}}{\ln(T_{\mathrm{tube}} - T_{f,\mathrm{in}})/(T_{\mathrm{tube}} - T_{f,\mathrm{out}})},$$

making the assumption that the inlet and outlet temperatures of the coolant in the tube are equal to the tube temperature. $T_{f,\mathrm{out}}$ is the fluid bulk temperature at the outlet section.

With the same assumption, the air side effectiveness of the heat exchanger is defined as:

$$\varepsilon = \frac{T_{f,\mathrm{out}} - T_{f,\mathrm{in}}}{T_{\mathrm{tube}} - T_{f,\mathrm{in}}} \tag{11}$$

The entropy production number N_{S1} can be evaluated by taking into account all the local contributions:

$$N_{S1} = \frac{T_{f,\mathrm{in}}.N_\beta \int \dot{S}'''\, dV}{N_\beta \Phi} = \frac{T_{f,\mathrm{in}}\dot{S}}{\Phi} \tag{12}$$

where N_β is the number of finned oval tube elements for a heat exchanger and $\dot{S} = \int \dot{S}'''\, dV$ is the entropy production rate computed for a finned oval tube element.

The results show that the effectiveness increases with Fi and β. Moreover, as expected for a $Be \sim 1$, the NTU increases

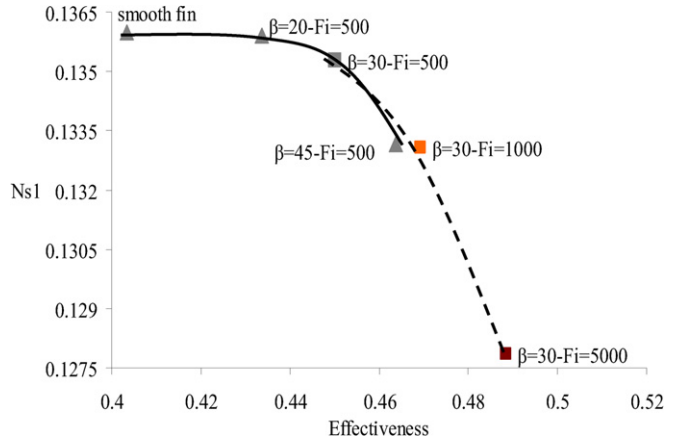

Fig. 15. Evolution of N_{S1} versus effectiveness. Square symbols and doted line: variation of *Fi*, Tri symbols and plain line: variation of β.

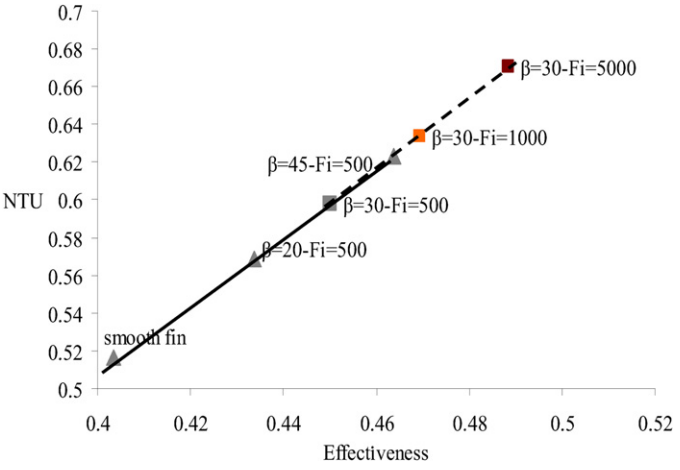

Fig. 16. Evolution of N_{S1} versus NTU. Square symbols and doted line: variation of *Fi*, Tri symbols and plain line: variation of β.

with the heat exchanger effectiveness whereas N_{S1} decreases (Figs. 15 and 16). The hierarchies of the heat exchanger performances are identical with both methodologies. Thus, the same kind of analysis can be performed with both approaches. The heat load of a component increases with β and *Fi* because of an increase of surface heat transfer coefficient and the fin efficiency respectively. In order to reach the technical requirement, the number of elements, thus the heat transfer surface of the exchanger, decreases with β and *Fi*. Therefore the heat transfer surface decreases with an increase of NTU but with a decrease of N_{S1}. In other words, for the heat exchangers considered which have the same heat load, the entropy production decrease with β and *Fi*.

Although the same global analysis can be done with the NTU method and the second law analysis, one can note some differences. In fact, in the case of fin made of aluminium ($Fi = 500$), for the first law there is a noticeable difference (9%) for the NTU values between the smooth fin and the fin with the delta winglet $\beta = 20°$, whereas for the second approach, the difference between both N_{S1} values is lower than 0.1%. The difference for N_{S1} become noticeable from the delta winglet angle $\beta = 30°$. The entropy minimization principle point of view, it means that there is not an improvement from the smooth fin to the fin with the delta winglet $\beta = 20°$.

For the cases ($\beta = 45°$, $Fi = 500$) and ($\beta = 30°$, $Fi = 1000$) the entropy production number is rather the same. The choice for an optimal design could be done if other technical requirements are specified, as, for example, the cost or the pressure drop. If the cost is a constraint the configuration ($\beta = 45°$, $Fi = 500$) should be chosen because of the higher copper ($Fi = 1000$) cost. If the pressure drop is the constraint, the configuration ($\beta = 30°$, $Fi = 1000$) should be used because of lower viscous dissipation. This simple example shows the interest to use the second law as a complementary tool to design heat exchangers. These first results are going to be extended in the future to other heat fin configurations and to other technical requirements.

6. Conclusions

A numerical evaluation of entropy production rate terms has been performed for the case of a finned oval tube with a punched longitudinal vortex generator in form of delta winglet.

The velocity and thermal gradients are both mechanisms of entropy production. The entropy production rate due to heat transfer and viscous dissipation occurs mainly in the down-wash zones where the boundary layer is thin. On the contrary, in the up-wash zones where the boundary layer is thick, the entropy production rate is smaller than in down-wash zones due to the weaker gradients. The outer surface of the longitudinal vortex is also a zone of entropy production and should be taken into account in the global evaluation. The entropy production rate due to thermal gradient is predominant for such a configuration.

The influence of the delta winglet angle (β) and the fin efficiency parameter (*Fi*) has been evaluated using the entropy production rate. The increase of the angle β of the delta winglet leads to an increase of the viscous entropy production in the fluid and of an increase of the thermal entropy production in the flow field and in the fin. A better fin efficiency is responsible of a decrease of entropy in the fin but it is widely balanced by entropy generation rate in the fluid.

The integration of the local information allows us to define the global second law heat exchanger criterion N_{S1} proposed by Hesselgreaves [5]. When the effectiveness increases, the NTU increases, but the entropy production number N_{S1} decreases.

Moreover, NTU is established under strong assumptions. In fact the logarithm difference temperature definition used to model the global heat transfer coefficient assumes that the heat transfer coefficient is constant on the surface, which is clearly not the case because of the vortex generator. On the contrary, the entropy production rate does not suffer any additional modeling or other assumptions, being an integration of all local contributions.

Entropy production was found to be useful to study local conjugate heat transfer and to define a global heat exchanger criterion. The entropy production number proves to be a successful tool to analyze exchange surfaces and should be an

efficient complementary tool for engineers when designing heat exchangers.

Acknowledgements

This work was supported by the French National Agency for Research and Technology (ANRT) and Valeo Engine Cooling. Both are gratefully acknowledged.

References

[1] A. Bejan, Entropy Generation Minimization, CRC Press, Boca Raton, 1996.
[2] D.P. Sekulic, Entropy generation in a heat exchanger, Heat Transfer Engineering 7 (1–2) (1986) 83–88.
[3] D.P. Sekulic, C.V. Herman, One approach to irreversibility minimization in compact crossflow heat exchanger design, Int. Com. Heat Mass Transfer 13 (1986) 23–32.
[4] M. Yilmaz, O.N. Sara, S. Karoli, Performance evaluation criteria for heat exchangers based on second law analysis, Exergy Int. J. 1 (4) (2001) 278–294.
[5] J.E. Hesselgreaves, Rationalisation of the second law analysis of heat exchangers, Int. J. Heat Mass Transfer 43 (2000) 4189–4204.
[6] D. Poulikakos, A. Bejan, Fin geometry for minimum entropy generation in forced convection, Trans. ASME 104 (1982) 616–623.
[7] A. Datta, Effects of gravity on structure and entropy generation of confined laminar diffusion flames, Int. J. Thermal Sci. 44 (5) (2005) 429–440.
[8] S. Mahmud, R.A. Fraser, Flow, thermal, and entropy generation characteristics inside a porous channel with viscous dissipation, Int. J. Thermal Sci. 44 (1) (2005) 21–32.
[9] F. Kock, H. Herwig, Entropy production calculation for turbulent shear flows and their implementation in CFD codes, Int. J. Heat Mass Transfer 26 (2005) 672–680.
[10] T.H. Ko, Numerical analysis of entropy generation and optimal Reynolds number for developing laminar forced convection in double-sine ducts with various aspect ratios, Int. J. Heat Mass Transfer 49 (3–4) (2006) 718–726.
[11] T.H. Ko, K. Ting, Entropy generation and optimal analysis for laminar forced convection in curved rectangular ducts: A numerical study, Int. J. Thermal Sci. 45 (2) (2006) 138–150.
[12] T.H. Ko, Numerical investigation on laminar forced convection and entropy generation in a curved rectangular duct with longitudinal ribs mounted on heated wall, Int. J. Thermal Sci. 45 (4) (2006) 390–404.
[13] T.H. Ko, A numerical study on entropy generation and optimization for laminar forced convection in a rectangular curved duct with longitudinal ribs, Int. J. Thermal Sci. 45 (11) (2006) 1113–1125.
[14] T.H. Ko, A numerical study on developing laminar forced convection and entropy generation in half- and double-sine ducts, Int. J. Thermal Sci. 46 (12) (2007) 1275–1284.
[15] E. Sciubba, A minimum entropy generation procedure for the discrete pseudo-optimization of finned tube heat exchangers, Revue Générale de Thermique 35 (1996) 517–525.
[16] J. Herpe, D. Bougeard, S. Russeil, B. Baudoin, Numerical investigation of entropy generation in the case of finned oval tube with a punched longitudinal vortex generator in form of delta winglet, in: ASME Joint US–European Fluids Engineering Summer Meeting, 2006, July 17–20, Miami, FL, FEDSM2006-98393.
[17] J. Herpe, S. Russeil, D. Bougeard, Numerical analysis of entropy production of louvered fin heat exchanger, in: Sixth Int. Conf. on Enhanced, Compact and Ultra-Compact Heat Exchanger: Science, Engineering and Technology, September 2007, Potsdam, Germany, CD-ROM, N°CHE2007-0021, pp. 149–154.
[18] P. Eibeck, An experimental investigation of the heat transfer effects of a longitudinal vortex embedded in a turbulent boundary layer, PhD thesis, Department of Mechanical Engineering, Stanford University, 1985.
[19] W.R. Pauley, The fluid dynamics and heat transfer effects of streamwise vortices embedded in a turbulent boundary layer, PhD thesis, Department of Mechanical Engineering, Stanford University, 1988.
[20] Y. Chen, M. Fiebig, N.K. Mitra, Conjugate heat transfer of a finned oval tube with a punched longitudinal vortex generator in form of delta winglet-parametric investigations of the winglet, Int. J. Heat Mass Transfer 41 (1998) 3961–3978.
[21] Y. Chen, M. Fiebig, N.K. Mitra, Heat transfer enhancement of a finned oval tube with punched longitudinal vortex generators in-line, Int. J. Heat Mass Transfer 41 (1998) 4151–4166.
[22] Y. Chen, M. Fiebig, N.K. Mitra, Heat transfer enhancement of finned oval tubes with staggered punched longitudinal vortex generators, Int. J. Heat Mass Transfer 43 (2000) 417–435.
[23] M. Fiebig, A. Grosse-Gorgemann, Y. Chen, N.K. Mitra, Conjugate heat transfer of a finned tube. Part A: Heat transfer behavior and occurrence of heat transfer reversal, Numer. Heat Transfer A 28 (1995) 133–146.
[24] M. Fiebig, Y. Chen, A. Grosse-Gorgemann, N.K. Mitra, Conjugate heat transfer of finned tube. Part B: Heat transfer augmentation and avoidance of heat transfer reversal by longitudinal vortex generators, Numer. Heat Transfer A 28 (1995) 147–155.
[25] D. Tiwari, D. Mauya, G. Biswas, V. Eswaran, Heat transfer enhancement in cross-flow heat exchangers using oval tubes and multiple delta winglets, Int. J. Heat Mass Transfer 46 (2003) 2841–2856.
[26] G. Biswas, K. Torii, D. Fujii, K. Nishino, Numerical and experimental determination of flow structure and heat transfer effects of longitudinal vortices in a channel flow, Int. J. Heat Mass Transfer 39 (16) (1996) 3441–3451.
[27] K. Torii, K.M. Kwak, K. Nishino, Heat transfer enhancement accompanying pressure loss reduction with winglet type vortex generators for fin tube heat exchangers, Int. J. Heat Mass Transfer 45 (2002) 3795–3801.
[28] F. Kock, Bestimmung der lokalen entropieproduktion in turbulenten strömungen und deren Nutzung zur bewertung konvektir transportprozesse, PhD thesis, TU Hamburg-Harburg, 2003.
[29] J. Moore, J.G. Moore, Entropy production rate from viscous flow calculations. Part 1. A turbulent boundary layer flow, Transaction of the ASME, 83-GT-70.
[30] O.B. Adeyinka, G.F. Naterer, Modelling of entropy production in turbulent flows, J. Fluids Engineering 126 (2004) 893–899.
[31] Fluent User's guide. Version 6.2, Fluent, Inc., 2005.
[32] J. Herpe, Caractérisation des performances des surfaces d'échange basée sur l'évaluation numérique du taux de production d'entropie : Application aux échangeurs de chaleur d'automobiles, Thèse de doctorat, Université de Valenciennes et du Hainaut Cambrésis, 2007.
[33] R.R. Mendez, M. Sen, K.T. Yang, R. McClain, Effect of fin spacing on convection in plate fin and tube heat exchanger, Int. J. Heat Mass Transfer 3 (1) (2000) 39–51.
[34] F.P. Incropera, D.P. DeWitt, Fundamental of Heat and Mass Transfer, fourth ed., Wiley, 1996.